Supporting Information for:

Trapping of a putative intermediate in the cytochrome *c* nitrite reductase (ccNiR)-catalyzed reduction of nitrite: implications for the ccNiR reaction mechanism

Mahbbat Ali, Natalia Stein, Yingxi Mao, Shahid Shahid, Marius Schmidt, Brian Bennett, and A. Andrew Pacheco

S1. Verification of ccNiR purity by SDS-PAGE

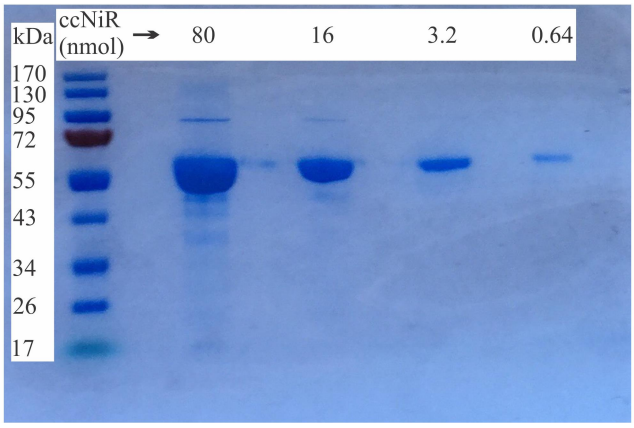

Figure S1. Typical SDS-PAGE for pure ccNiR samples used in the experiments described herein.

S2. *S. oneidensis* CcNiR structure refinement

The new structure of *S. oneidensis* ccNiR was refined with "phenix", and using the structural validation tools implemented in 'coot'. Figure S2a shows the structural validation at a glance using the 'polygon' validation tool implemented in 'phenix'.[2] Data statistics and the result of the refinement are shown in Table S1. The electron density is of excellent quality. Slight structural mismatches in our earlier 2.59 Å Laue structure (3UBR) were successfully modeled at 1.66 Å. We then re-interpreted the published Laue data with the new model with essentially the same refinement protocol as reported above. R/R-free values reported in the earlier publication[1] dropped from 19.7/25.7 to 16.0/24.2, respectively. The result from the 'polygon' validation tool is shown in Fig. S2b. Geometry measurements (distances and angles) were performed with 'coot' and are reported in Table S2. The relative angles of the proximal

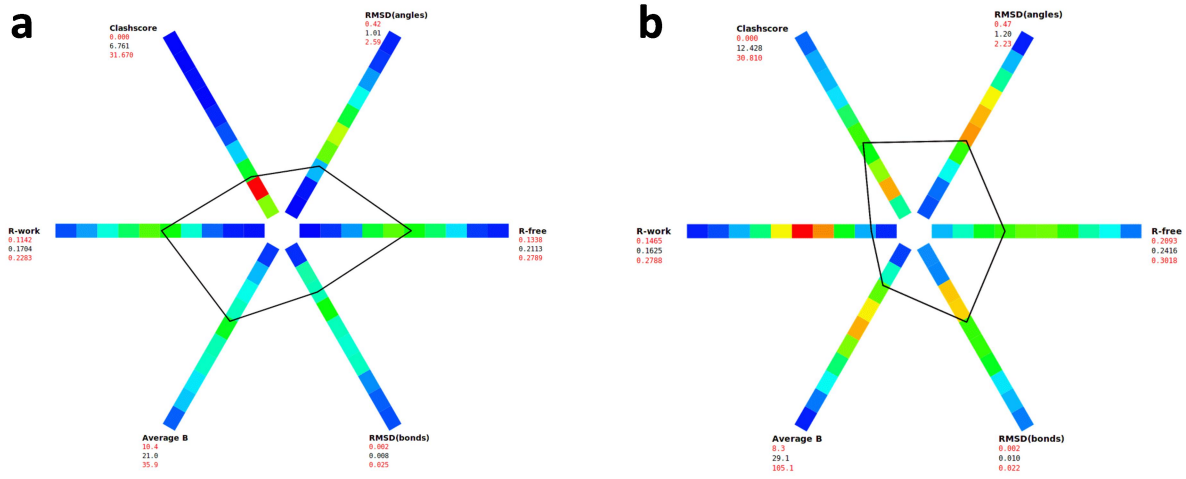

Figure S2. Structure validation polygons from the refinement of the *S. oneidensis* ccNiR. Green colors: parameters frequently found in structures at similar resolution. Blue colors: parameters less frequently found. All parameters are well within the range expected from the resolution of the data. (a) 1.66 Å cryo-structure (this work). (b) 2.59 Å room temperature Laue structure.[1]

and distal histidines were determined as torsional angles using two equivalent atoms in each histidine ring. This provides approximate angles, since the histidine ring surfaces are essentially aligned along the same axis.

Figure S3 compares the structure of the *S. oneidensis* active site region as obtained in the current study at 110 K, with that obtained previously at room temperature using the Laue method.[1] The two structures are seen to be very comparable, showing that neither difference in the temperature of data collection, nor purification method, had a significant impact. The structures obtained by the two methods were similarly homologous throughout the remainder of the protein, in both protomers.

Table S1. Statistics of X-ray data collection and refinement. Numbers in brackets: highest resolution shell.

	X-ray Data
Resolution	1.66 Å
Temperature	110 K
Space group	$P2_12_12_1$
Unit-cell parameters (Å,°)	a = 50.2 b = 96.1 c=222.6 α=90 β=90 γ=90
Observations	385,349
No of unique reflections	97,476
Redundancy	4.1
Completeness (%)	76.3
CC1/2*	0.991 (0.78)
R_{merge} (%)	9.0 (48.1)
mosaicity (°)	0.25
	Model Building Refinement
R_{cryst}/R_{free} (%)	17.1/21.8
# subunit/asu	2
# residues/subunit	428
# water	1314
room mean square deviation of bonds (Å)/angles (°)	0.013/1.010
Ramachandran outliers	1

*correlation coefficient in resolution shells between data in a dataset of multiple observations split in half.

Table S2. Heme iron axial ligand geometry for subunits A and B of the *S. oneidensis* ccNiR. The axial ligands of heme 1 are the distal water and Lys-123, those of all other hemes are histidines. The axial angle is formed either by water, oxygen, the iron and the Nz of Lys-123, or by the NE atoms of the axial histidine ligands and the heme iron. The relative angles of the histidine ring surface normals are also shown.

	Heme 1	**Heme 2**	**Heme 3**	**Heme 4**	**Heme 5**
	high resolution (1.66 Å), cryo structure				
Fe-Ligand1	H_20/2.33	HisNE/2.00	HisNE/2.03	HisNE/2.06	HisNE/2.05
Fe-Ligand2	LysNZ/2.08	HisNE/2.08	HisNE/2.04	HisNE/2.10	HisNE/2.04
axial angle	168°	175°	175°	178°	180°
relative histidine ring angle	nd	24°	45°	77°	85°
Fe-Ligand1	H_20/2.38	HisNE/2.00	HisNE/1.96	HisNE/2.01	HisNE/2.06
Fe-Ligand2	LysNZ/2.07	HisNE/2.06	HisNE/2.08	HisNE/2.08	HisNE/2.02
axial angle	168°	178°	174°	176°	178°
relative histidine ring angle	nd	8°	36°	68°	88°
	medium resolution (2.59 Å), room temperature Laue structure.[1]				
Fe-Ligand1	H_20/2.66	HisNE/1.97	HisNE/1.91	HisNE/1.94	HisNE/2.07
Fe-Ligand2	LysNZ/2.19	HisNE/1.92	HisNE/2.12	HisNE/2.03	HisNE/2.00
axial angle	164°	171°	166°	173°	175°
Relative histidine ring angle	nd	19°	55°	81°	84°
Fe-Ligand1	H_20/2.54	HisNE/1.85	HisNE/2.22	HisNE/1.92	HisNE/2.18
Fe-Ligand2	LysNZ/2.32	HisNE/2.01	HisNE/2.03	HisNE/2.03	HisNE/2.02
axial angle	162°	177°	176°	174°	172°
relative histidine ring angle	nd	10°	39°	75°	89°

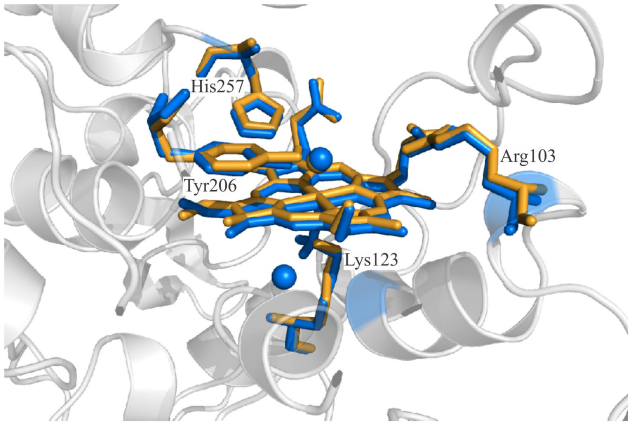

Figure S3. Comparison of the *S. oneidensis* ccNiR active site region structures as obtained in the current study at 110 K (blue), and previously at room temperature using the Laue method (orange).[1] The figure shows the active site heme 1, its unusual proximal ligand Lys123, three conserved active site ligands believed to be catalytically important, the water coordinated to the distal site of heme 1 in the resting enzyme, and a water that hydrogen bonds to Lys 123.

S3. Mediators used for spectropotentiometric experiments

Table S3. Mediators used for spectropotentiometry

Mediator	$\varepsilon_{0.5}$ (V vs SHE)	Used for	Concentration (μM)
N,N,N′,N′-tetramethyl-*p*-phenylenediamine	0.26[a,b]	UV/Vis	25
1,2-naphthoquinone-4-sulfonic acid	0.168[a]	UV/Vis, EPR	100
Phenazine methosulfate	0.08[b]	UV/Vis	25
Hexaammineruthenium(III) chloride	–0.02[a]	UV/Vis	100

[a] These midpoint potentials were obtained or verified in-house, at pH 7, using UV/Vis spectropotentiometry or cyclic voltammetry

[b] Obtained from ref. 6

Table S3 lists all of the mediators that were used to investigate the electrochemical properties of nitrite-loaded ccNiR. In practice most of these were used only in preliminary studies, when we had yet to determine even the approximate value of the $Fe_{H1}^{III}(NO_2^-)$ midpoint potential. Once the midpoint potential range was established, the mediator soup was trimmed to two components: *N,N,N′,N′*-tetramethyl-*p*-phenylenediamine (TMPD) and 1,2-naphthoquinone-4-sulfonic acid. For all the experiments reported in the main body of the paper the soup was further trimmed to the single mediator 1,2-naphthoquinone-4-sulfonic acid. This didn't significantly affect the measured midpoint potential, and was convenient because at 100 μM in a 0.02 cm path cell 1,2-naphthoquinone-4-sulfonic acid reduction is accompanied by very small absorbance changes above 350 nm. Figure S5 shows the extinction coefficient difference spectrum associated with 1,2-naphthoquinone-4-sulfonic acid reduction (Fig. S5a), and the absorbance change expected upon reduction of 100 μM of the mediator (Fig. S5b). The difference spectrum has no sharp features, and the biggest change (at 400 nm) is less than 5 mAU. Spectral changes associated with TMPD oxidation were also small (about 5 mAU at both 563 nm and 612

nm, Fig. S4), but the $TMPD^+$ spectral features are a lot sharper and more distinct. Consequently the $TMPD^+$ spectral contribution, though minor, was typically subtracted at each applied potential (reduced TMPD itself doesn't absorb in the visible range). Similarly the spectral contributions from phenazine methosulfate, which were substantially higher than those of either $TMPD^+$ or 1,2-naphthoquinone-4-sulfonic acid, and also displayed a sharp feature in the Soret region (Fig. S6), were always subtracted at each applied potential. Neither oxidized nor reduced hexaammineruthenium chloride absorb appreciably above 350 nm.

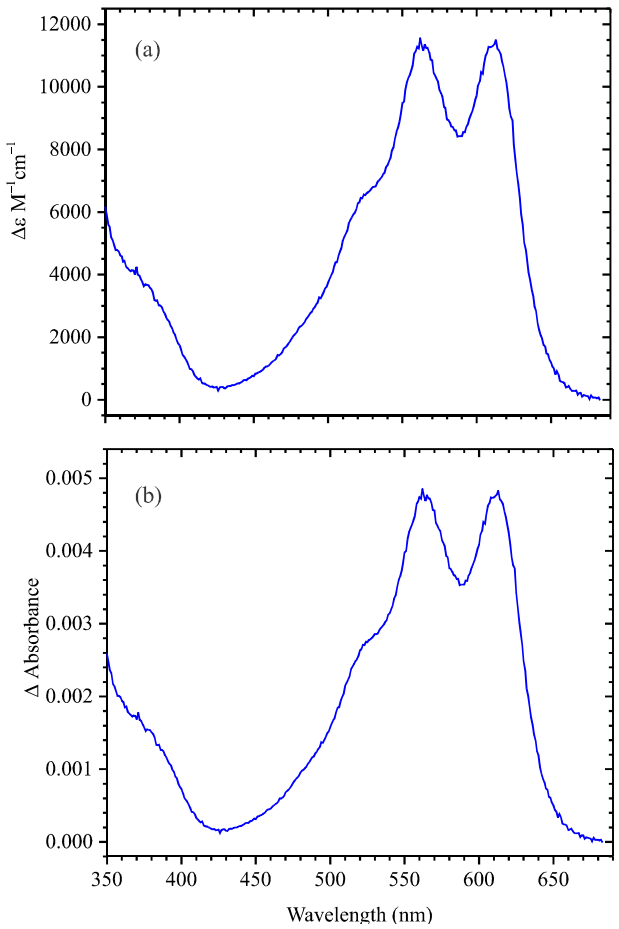

Figure S4. (a) Extinction coefficient difference spectrum for reduced – oxidized *N,N,N',N'*-tetramethyl-*p*-phenylenediamine (ΔTMPD; only the oxidized form absorbs in the region from 350 nm – 800 nm) . (b)Spectral contribution expected from 25 μM ΔTMPD, contained in a 0.02 cm pathlength cuvette.

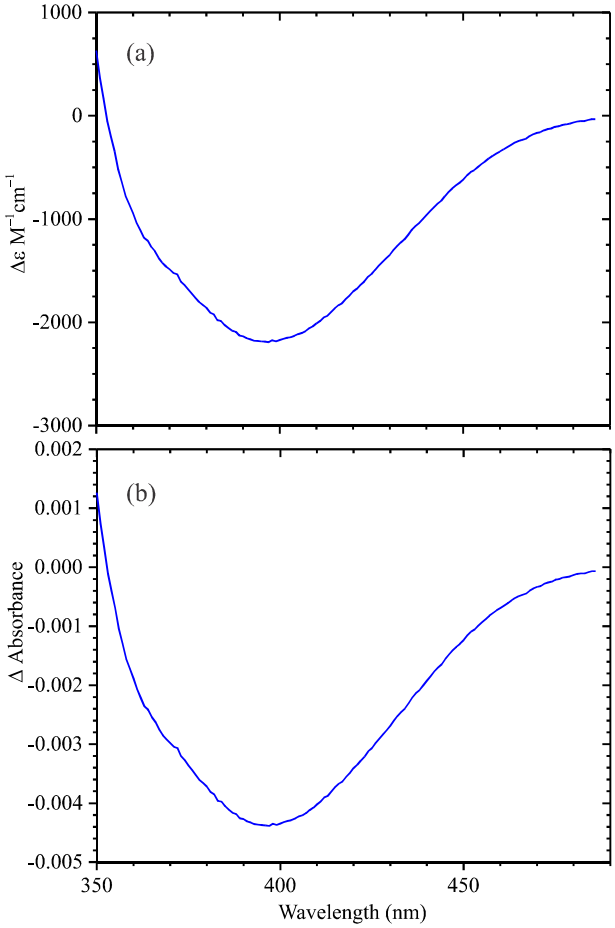

Figure S5. (a) Extinction coefficient difference spectrum for reduced – oxidized 1,2-naphthoquinone – 2-sulfonic acid (ΔNPSA; only the oxidized form absorbs in the region from 350 nm – 500 nm, neither form absorbs above 500 nm). (b) Spectral contribution expected from 100 μM ΔNPSA, contained in a 0.02 cm pathlength cuvette.

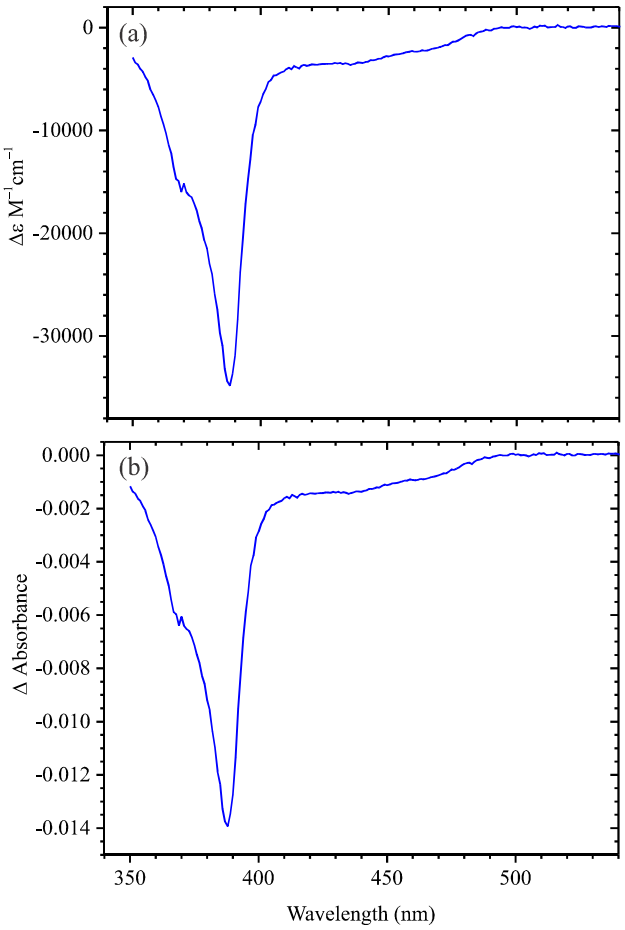

Figure S6. (a) Extinction coefficient difference spectrum for reduced – oxidized Phenazine methosulfate (ΔPMS; only the oxidized form absorbs in the region from 350 nm – 500 nm, and neither form absorbs above 500 nm). (b) Spectral contribution expected from 25 μM ΔPMS, contained in a 0.02 cm pathlength cuvette.

S4. Equilibrium expression for nitrite binding to the ccNiR active site

In this section and the next we will refer to Scheme 2 from the main text, reproduced as Scheme S1 below. The first step in Scheme S1 describes the binding of nitrite to the ferriheme ccNiR active site (Fe_{H1}^{III}), and is governed by the binding constant K, as shown in Eq. S1. This is the topic of this Section. The relationship between nitrite binding and subsequent reduction of $Fe_{H1}^{III}(NO_2^-)$ will be discussed in Section S5.

$$Fe_{H1}^{III} + NO_2^- \overset{K}{\rightleftharpoons} Fe_{H1}^{III}(NO_2^-) \qquad (1)$$

$$Fe_{H1}^{III}(NO_2^-) + 2e^- + 2H^+ \overset{\varepsilon^\circ}{\rightleftharpoons} \{Fe_{H1}NO\}^7 + H_2O \qquad (2)$$

$$\{FeNO\}^7 = [Fe^{II}(NO\cdot) \longleftrightarrow Fe^{III}(NO^-)]$$

Scheme S1.

$$K = \frac{[Fe_{H1}^{III}(NO_2^-)]}{[Fe_{H1}^{III}][NO_2^-]} \qquad \text{S1}$$

During a titration of ccNiR by nitrite we will define the total ccNiR concentration as Fe_T, and the total nitrite concentration at any given titration step as N_T. Thus, at any given titration step, the distributions of ccNiR and nitrogenous species in solution are given by Eqs. S2 and S3, respectively.

$$Fe_T = [Fe_{H1}^{III}] + [Fe_{H1}^{III}(NO_2^-)] \qquad \text{S2}$$

$$N_T = [NO_2^-] + [Fe_{H1}^{III}(NO_2^-)] \qquad \text{S3}$$

Solving Eqs S2 and S3 for $[Fe_{H1}^{III}]$ and $[NO_2^-]$, respectively, and substituting into Eq. S1, yields expression S4. This in turn can be solved for $[Fe_{H1}^{III}(NO_2^-)]$ to give Eq. 2 from the main text.

$$K = \frac{[Fe_{H1}^{III}(NO_2^-)]}{\{Fe_T - [Fe_{H1}^{III}(NO_2^-)]\}\{N_T - [Fe_{H1}^{III}(NO_2^-)]\}} \qquad \text{S4}$$

$$[Fe_{H1}^{III}(NO_2^-)] = \frac{(Fe_T + N_T)\cdot K + 1 - \sqrt{Fe_T^{\,2}\cdot K^2\cdot N_T + 2Fe_T\cdot K + K^2\cdot N_T^{\,2} + 2K\cdot N_T + 1}}{2K} \qquad \text{Eq.2}$$

S5. Dependence of nitrite-loaded ccNiR's electrochemical behavior on pH and nitrite concentration

Equation S5 is the Nernst equation associated with reaction (2) of Scheme S1. In Eq. S5 ε_{app} is the potential applied during the spectropotentiometric experiment, and ε^{o} is the standard reduction

$$\varepsilon_{app} = \varepsilon^{o} - \frac{RT}{2F}\ln\frac{\{Fe_{H1}NO\}^{7}}{[Fe^{III}_{H1}(NO_2^-)][H^+]^2} \qquad \text{S5}$$

potential. In a buffered solution Eq. S5 can be rearranged to the form S6, which defines the apparent midpoint potentials $\varepsilon^{o}_{\mathrm{pH}}$ that will be obtained in spectropotentiometric experiments at varying pHs.

$$\varepsilon_{app} = \varepsilon^{o}_{pH} - \frac{RT}{2F}\ln\frac{\{Fe_{H1}NO\}^{7}}{[Fe^{III}_{H1}(NO_2^-)]} \qquad \text{S6}$$

where

$$\varepsilon^{o}_{pH} = \varepsilon^{o} - \frac{2.303RT}{F}pH$$

Equation S6 is readily rearranged to the exponential form S7, which is more appropriate for fitting results from experiments in which ε_{app} is the independent variable.

$$\frac{\{Fe_{H1}NO\}^{7}}{[Fe^{III}_{H1}(NO_2^-)]} = \exp\left[\frac{2F}{RT}\left(\varepsilon^{o}_{pH} - \varepsilon_{app}\right)\right] \qquad \text{S7}$$

When the nitrite concentration is high, equilibrium 1 in Scheme S1 will lie far to the right, so the concentration of ccNiR without nitrite in the active site ($[Fe_{H1}{}^{III}]$) will be negligible. The exponential Nernst equation can then be written as Eq.S8.

$$\{Fe_{H1}NO\}^{7} = \frac{Fe_T \cdot \exp\left[\frac{2F}{RT}\left(\varepsilon^{o}_{pH} - \varepsilon_{app}\right)\right]}{1 + \exp\left[\frac{2F}{RT}\left(\varepsilon^{o}_{pH} - \varepsilon_{app}\right)\right]} \qquad \text{S8}$$

where

$$Fe_T = [Fe^{III}_{H1}(NO_2^-)] + \{Fe_{H1}NO\}^{7}$$

In our UV/Vis spectropotentiometric experiments we monitored spectral changes as a function of the applied potential. To relate the Nernst equation with spectral changes at a given applied potential ε_{app} we use Beer's law (Eq. S9), in which $\epsilon_{1\lambda}$ and $\epsilon_{2\lambda}$ are the extinction coefficients of $[Fe_{HI}{}^{III}(NO^{2-})]$ and

$$A_{\lambda,\varepsilon_{app}} = \left(\epsilon_{1\lambda}[Fe^{III}_{H1}(NO_2^-)]_{\varepsilon_{app}} + \epsilon_{2\lambda}\{Fe_{H1}NO\}^{7}_{\varepsilon_{app}}\right)\cdot l \qquad \text{S9}$$

$\{Fe_{HI}NO\}^{7}$, respectively, at wavelength λ. For difference spectra Eq. S9 can be recast in the form S10, where $\Delta\epsilon_\lambda = \epsilon_{2\lambda} - \epsilon_{1\lambda}$, and $\Delta A_{\lambda,\varepsilon app} = A_{\lambda,\varepsilon app} - A_{o\lambda,\varepsilon app}$; $A_{o\lambda,\varepsilon app}$ is the absorbance of the fully oxidized ccNiR (obtained in the absence of an applied potential). Finally, Eqs. S8 and S10 can be combined to give, after some rearrangement, Eq. S11.

$$\{Fe_{H1}NO\}^{7}_{\varepsilon_{app}} = \frac{\Delta A_{\lambda,\varepsilon_{app}}}{\Delta\epsilon_\lambda \cdot l} \qquad \text{S10}$$

$$\Delta A_{\lambda,\varepsilon_{app}} = \frac{Fe_T \cdot \Delta\epsilon_\lambda \cdot l \cdot \exp\left[\frac{2F}{RT}\left(\varepsilon^o_{pH} - \varepsilon_{app}\right)\right]}{1+\exp\left[\frac{2F}{RT}\left(\varepsilon^o_{pH} - \varepsilon_{app}\right)\right]} \qquad \text{S11}$$

Equation S11 is identical in form to Eq. 3 from the main text, and at limiting nitrite concentrations the empirical parameter $\varepsilon_m{}^o$ of Eq. 3 can be interpreted to be $\varepsilon^o{}_{pH}$ as defined in Eq. S6. Also, $\Delta A_{max(\lambda)}$ of Eq. 3 will correspond with the product $Fe_T \cdot \Delta\epsilon_\lambda \cdot l$ of Eq. S11. Since the pathlength and total ccNiR concentration Fe_T were known for all experiments, an extinction coefficient difference spectrum corresponding to reduction of the oxidized protein to the 2-electron reduced $\{Fe_{H1}NO\}^7$ form was obtained from experiments carried out in the presence of high nitrite concentrations (Fig. S7). This difference spectrum could then be used to determine the extent of ccNiR reduction under conditions when full reduction was not necessarily achieved (see below and main text). Finally, the extinction coefficient difference spectrum of Fig. S7, together with the independently obtained extinction coefficient spectrum of fully oxidized ccNiR, could be used to obtain the absolute spectrum of $\{Fe_{H1}NO\}^7$ ccNiR. This spectrum is shown in Fig. S8; the spectrum of the oxidized species is shown for comparison. The $\{Fe_{H1}NO\}^7$ ccNiR extinction coefficient spectrum was used to fit the data shown in Fig. 7a of the main paper.

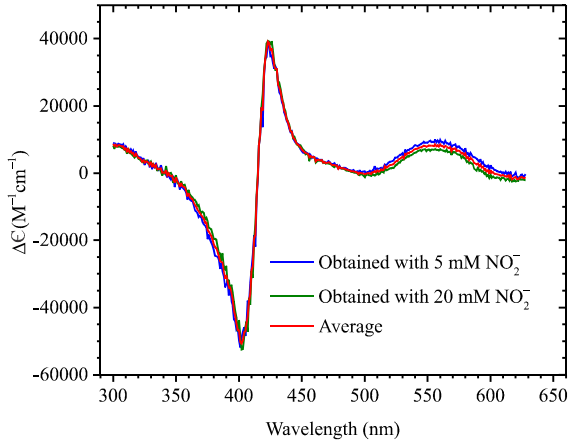

Figure S7. Extinction coefficient difference spectra obtained by fitting data collected in the presence of 5 mM (blue trace) and 20 mM (green trace) to Eq. S11. The red trace is the average of the other two, and was used to determine the extent of ccNiR reduction in experiments where this was not known apriori.

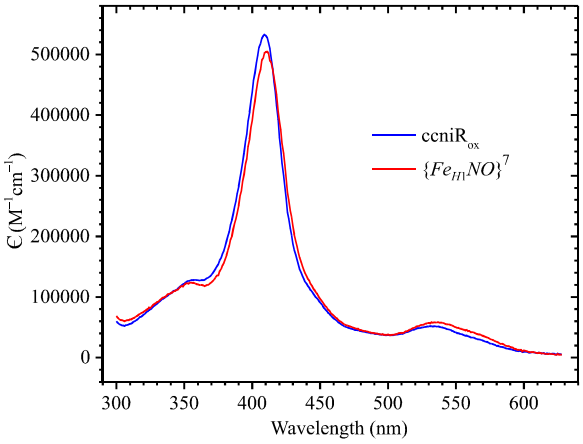

Figure S8. Red trace: extinction coefficient spectrum of $\{Fe_{H1}NO\}^7$ ccNiR. Blue trace: spectrum of fully oxidized ccNiR.

Equation 3 from the main text, an empirical Nernst equation in exponential form, was found to effectively model spectropotentiometric data sets collected for ccNiR in the presence of nitrite concentrations ranging from 20 mM, all the way down to 30 μM, which was sub-stoichiometric compared to the ccNiR concentration. However, the empirical parameter $\varepsilon_m{}^o$ of Eq. 3 can only be correlated with $\varepsilon^o{}_{pH}$ as defined in Eq. S6 under conditions in which ccNiR was saturated with nitrite. At lower nitrite concentrations Equilibrium (1) of Scheme S1 must be accounted for, as will be described next.

When ccNiR can exist in both nitrite-loaded and nitrite-free forms, the total ccNiR concentration will be given by Eq. S12. Equation S7 is still valid under these conditions, and it can be combined with Eq. S12 to eliminate the reduced species from the expression. This gives Eq. S13. At sufficiently low nitrite concentrations we also need to consider that an appreciable fraction of the nitrite added to the

$$Fe_T = [Fe^{III}_{H1}] + [Fe^{III}_{H1}(NO_2^-)] + \{Fe_{H1}NO\}^7 \quad \text{S12}$$

$$Fe_T = [Fe^{III}_{H1}] + [Fe^{III}_{H1}(NO_2^-)](1 + E1) \quad \text{S13}$$

where

$$E1 = \exp\left[\frac{2F}{RT}\left(\varepsilon^o_{pH} - \varepsilon_{app}\right)\right]$$

solution will end up bound to ccNiR. With this in mind we define N_T as the total concentration of nitrite that is initially added to the reaction mixture. Thus, at any given moment, the distribution of nitrogenous species will be given by Eq. S14. As with the expression for Fe_T above, Eqs. S14 and S7 can be combined to eliminate $\{Fe_{HI}NO\}^7$ from the expression (Eq. S15).

$$N_T = [NO_2^-] + [Fe^{III}_{H1}(NO_2^-)] + \{Fe_{H1}NO\}^7 \quad \text{S14}$$

$$N_T = [NO_2^-] + [Fe^{III}_{H1}(NO_2^-)](1 + E1) \quad \text{S15}$$

Combining Eqs. S1, S13 and S15 gives equilibrium expression S16, in which the only variable at a given ε_{app} is $[Fe^{III}_{H1}(NO_2^-)]$. Equation S16 is a quadratic, and can be solved for $[Fe^{III}_{H1}(NO_2^-)]$ (Eq. S17).

$$K = \frac{[Fe^{III}_{H1}(NO_2^-)]}{\left\{Fe_T - [Fe^{III}_{H1}(NO_2^-)]\cdot(1+E1)\right\}\left\{N_T - [Fe^{III}_{H1}(NO_2^-)]\cdot(1+E1)\right\}} \quad \text{S16}$$

$$[Fe^{III}_{H1}(NO_2^-)] = \frac{Fe_T \cdot K(1+E1) - \sqrt{Fe_T{}^2 \cdot K^2(1+E1)^2 - 2Fe_T \cdot K^2 \cdot N_T(1+E1)^2 + 2Fe_T \cdot K(1+E1) + K^2 \cdot N_T{}^2(1+E1)^2 + 2K \cdot N_T(1+E1)} + K \cdot N_T(1+E1) + 1}{2K(1+E1)^2} \quad \text{S17}$$

Once $[Fe_{H1}{}^{III}(NO^{2-})]$ has been obtained from Eq. S17, the corresponding concentration of $\{Fe_{H1}NO\}^7$ can be obtained straightforwardly with Eq. S18.

$$\{Fe_{H1}NO\}^7 = [Fe^{III}_{H1}(NO_2^-)] \cdot E1 \quad \text{S18}$$

In Eq. S17 the independent variable is the applied potential ε_{app} incorporated in $E1$ (Eq. S13). To use the equation $\varepsilon^o{}_{pH}$ (hidden in $E1$) was fixed at 0.246 V, the value obtained from spectropotentiometric titrations at pH 7 and saturating concentrations of nitrite (5 mM or higher), and the exact value of Fe_T was

determined in each experiment from the UV/Vis spectrum of the fully oxidized ccNiR prior to applying any potential. K was treated as an adjustable parameter, as described in the main text. For each trial K value Eqs. S17 and S18 were used to generate $[Fe_{H1}^{III}(NO^{2-})]$ and $\{Fe_{H1}NO\}^7$ vs. ε_{app} traces for the set of N_T values in Fig. 5 of the main text. The ε_m^o value at each N_T was then calculated as the value of ε_{app} at which $\{Fe_{H1}NO\}^7 = 0.5Fe_T$. Finally, the set of ε_m^o values obtained with Eqs. S17 and S18 were compared in a least-squares sense with those obtained using the empirical Eq. 3 from the main text, and K was adjusted to minimize the least-squares.

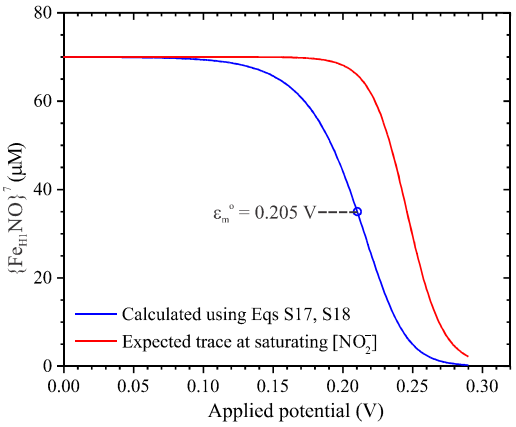

Figure S9. Blue trace: plot of $\{Fe_{H1}NO\}^7$ vs ε_{app} calculated using Eqs S17 and S18, when Fe_T and N_T are both 70 μM. The midpoint potential is taken as the value of ε_{app} at which 50% of Fe_T has been reduced. Red trace: plot obtained with N_T = 5 mM, when virtually all ccNiR is nitrite-loaded.

Figure S9 gives an example of a $\{Fe_{H1}NO\}^7$ vs ε_{app} trace generated with $Fe_T = N_T = 70$ μM; the trace that would be expected at saturating nitrite concentrations is also provided for comparison. The midpoint potential for the $\{Fe_{H1}NO\}^7$ vs ε_{app} trace is the point at which half the Fe_T (35 μM) has been reduced to $\{Fe_{H1}NO\}^7$; these are the calculated ε_m^o values plotted in Fig. 5 of the main text. Though the shapes of the plots obtained with Eqs S17, S18 at low N_T are not quite the same as the shapes generated by the empirical Nernst equation (Eq. 3, main text), the midpoint potentials obtained by fitting low N_T experimental data with the empirical equation tracked the ones calculated with Eqs S17 and S18 reasonably well (Fig. 5, main text).

S6. Spin quantitation of the nitrite-loaded ccNiR EPR spectrum after reduction

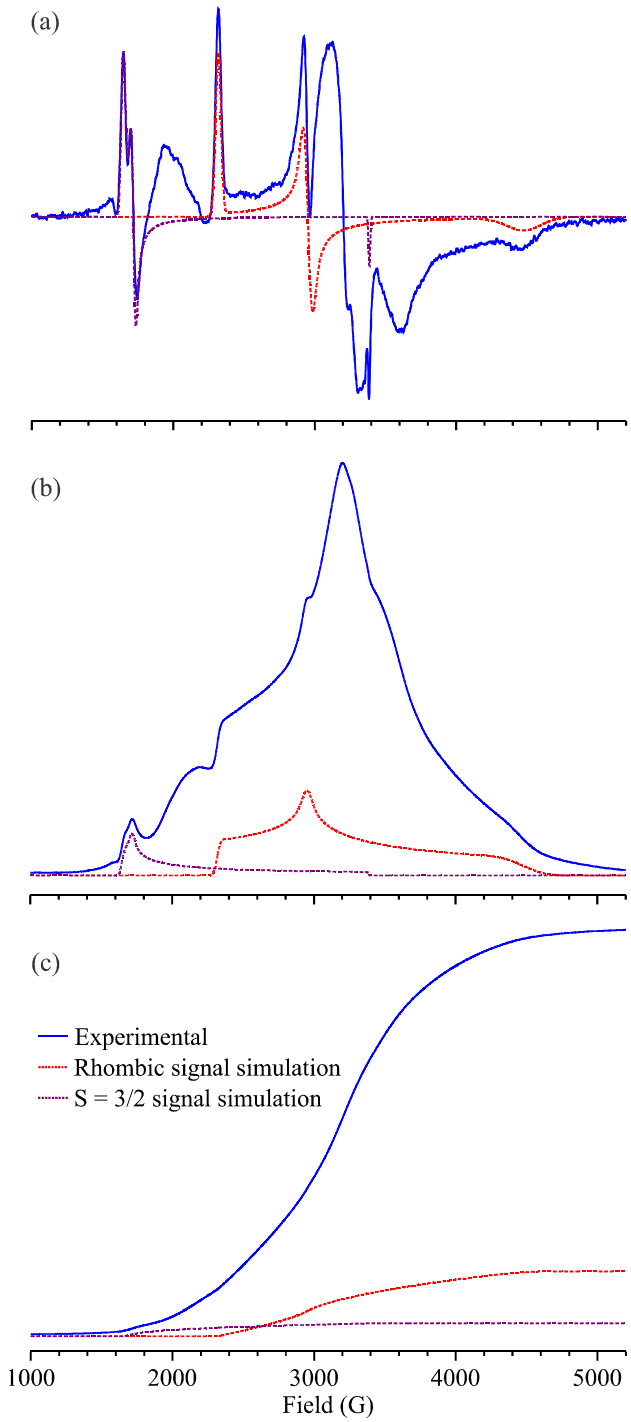

Figure S10. (a) Solid blue trace: X-band EPR spectrum of the nitrite-loaded ccNiR solution from Fig. 8 after reduction at $\mathcal{E}_{app}$ =160 mV vs SHE; dashed red trace: simulated spectrum of the rhombic signal arising from ccNiR heme 2; purple trace: simulation of the S = $^3/_2$ $\{FeNO\}^7$ signal. (b) Integration of the signals from (a). (c) Double integration.

The blue trace in Figure S10a shows the X-band EPR spectrum obtained for the solution from Fig. 8 of the main paper that initially contained 64 μM of fully oxidized ccNiR and 500 μM $^{14}NO_2^-$, after it was exposed to an applied potential of 160 mV vs SHE. The red dashed trace is a simulation of the rhombic signal previously assigned to ccNiR heme 2 (Fig. 1, main text),[7] while the purple dashed trace is a simulation of the $S = {}^3/_2$ $\{FeNO\}^7$ signal that appears as ccNiR is reduced. Figures S10b and S10c show the integrals and double integrals, respectively, of the Fig. S10a traces. The integrations show that the $S = {}^3/_2$ $\{FeNO\}^7$ signal has about 20% of heme 2's intensity. For the 64 μM ccNiR solution this would put the concentration of $S = {}^3/_2$ $\{FeNO\}^7$ at ~13 μM. The heme 2 signal in turn accounts for about 16% of the total spin envelope.

S7. Quantitation of adventitious iron in the EPR spectra

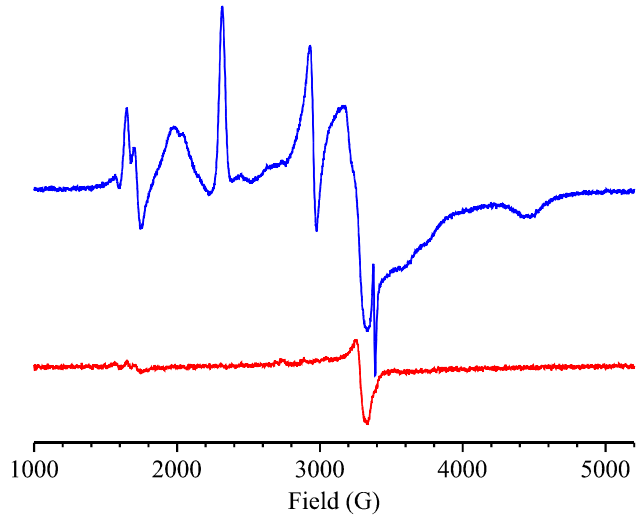

Figure S11. Blue trace: X-band EPR spectrum of the nitrite-loaded ccNiR solution from Fig. 8 after reduction at ε_{app} =160 mV vs SHE; Red trace: filtrate from ultrafiltration of a solution that initially contained the same species as those of Fig. 8, plus 25 μM Cu^{2+}, after adding approximately 60 μM $NO\cdot$, and subjecting it to an applied potential of 160 mV vs SHE.

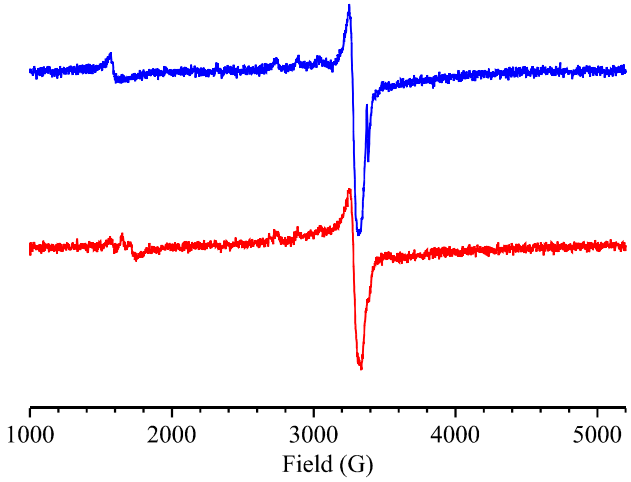

Figure S12. Blue trace: filtrate from ultrafiltration of a solution that initially contained the same components as those of Fig. 8, plus 25 μM Cu^{2+}, after adding approximately 60 μM $NO\cdot$, but before subjecting to a reducing potential. Red trace: same as red trace in Fig. S11.

The blue trace in Figure S11 shows the same EPR spectrum of reduced ccNiR as Fig. S10 and Fig. 8 from the main text. The red trace shows a spectrum for the filtrate from ultrafiltration of a solution that initially contained the same species as those that engendered the blue trace, plus 25 μM Cu^{2+} and 60 μM $NO\cdot$, and that was then subjected to an applied potential of 160 mV vs SHE. Spin quantitation of the red trace signals showed that the $S = {}^3/_2$ $\{FeNO\}^7$ signal's intensity was 0.75% that of the Cu^{2+}, which would amount to ~0.2 μM $\{FeNO\}^7$. For comparison, from the integration shown in Fig. S10 we estimated that the $S = {}^3/_2$ $\{FeNO\}^7$ signal was ~20% of heme 2 in a 64 μM ccNiR solution, which would come to ~13 μM $\{FeNO\}^7$.

Figure S12 compares the filtrate from ultrafiltration of the solution described for Fig. S11, before (blue trace) and after (red trace) subjecting it to the applied potential of 160 mV vs SHE. The rhombic ferric iron signal's intensity was found to be about 0.65% that of Cu^{2+} in the oxidized spectrum, which would amount to ~0.16 μM rhombic ferric iron, comparable to the concentration of $S = {}^3/_2$ $\{FeNO\}^7$ present after reduction (red trace); no $S = {}^3/_2$ signal was detectable in the filtrate prior to electrochemical reduction.

S8. Outlier result from an early experiment

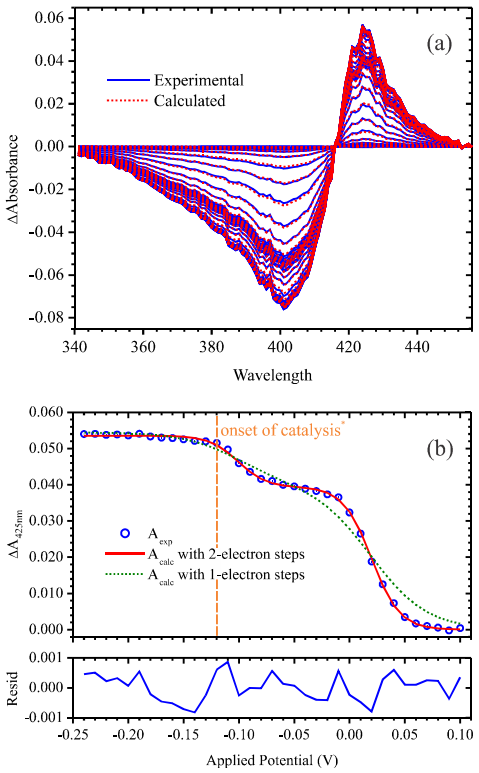

Figure S13. (a) UV/Vis spectral changes obtained in a single early experiment upon exposing a solution initially containing 58 μM of fully oxidized ccNiR and 5 mM nitrite to progressively lower potentials. Solid blue lines show the experimentally obtained data, whereas the dashed red lines were calculated from least-squares fitting with two Nernstian 2-electron reduction events and one spectral component; further details are available in ref. 3. The fit yields two midpoint potentials: $\mathcal{E}_{m1}{}^{o} = 0.02$ V, $\mathcal{E}_{m2}{}^{o} = -0.101$ V. (b) Blue circles: an absorbance difference vs. applied potential slice taken at 425 nm from the spectra of part (a); solid red line: least-squares best fit obtained from global analysis of the data with two Nernstian 2-electron reduction events; dotted green line: least-squares best fit obtained from global analysis of the same data with two Nernstian 1-electron reduction events.[3] The vertical dashed orange line shows approximately the applied potential above which no current for catalytic nitrite reduction is detected in protein film voltammetry experiments.[5]

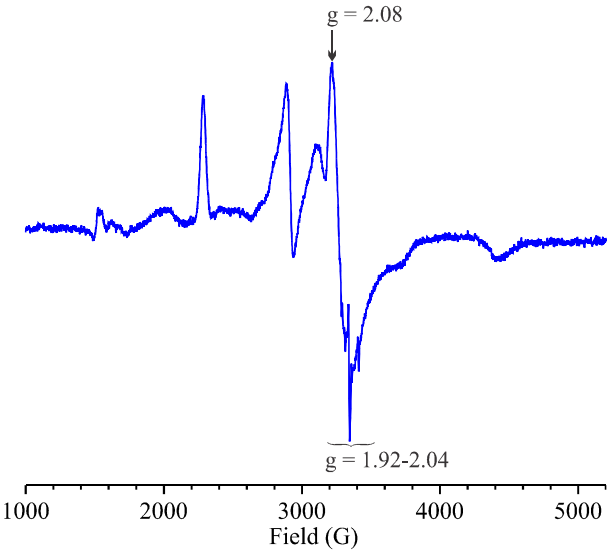

Figure S14. X-band EPR spectrum obtained in a single experiment, for a solution initially containing 50 μM of fully oxidized ccNiR and 5 mM nitrite, upon exposing it to an applied potential of –50 mV vs. SHE; experimental details are available in ref. 3. The labeled features are those that appear at positions typical of low-spin $\{FeNO\}^{7}$.[4]

Figures S13 and S14 show the results of a single set of UV/Vis- and EPR-spectropotentiometric experiments, performed with a single batch of ccNiR purified by the method of Youngblut et al,[1] that gave results different from the nearly two dozen spectro-potentiometric experiments carried out since, using multiple ccNiR batches purified either by the original Youngblut method,[1] or by the method described in the Materials and Methods section of the main document.

S8. References

(1) Youngblut, M.; Judd, E. T.; Srajer, V.; Sayyed, B.; Goelzer, T.; Elliott, S. J.; Schmidt, M.; Pacheco, A. A. Laue crystal structure of *Shewanella oneidensis* cytochrome *c* nitrite reductase from a high-yield expression system *J. Biol. Inorg. Chem.* **2012**, *17*, 647-662.

(2) Urzhumtseva, L.; Afonine, P. V.; Adams, P. D.; Urzhumtsev, A. Crystallographic model quality at a glance *Acta Cryst. D., Biol. Cryst.* **2009**, *65(Pt. 3)*, 297-300.

(3) Stein, N. Ph.D., University of Wisconsin-Milwaukee, Dept. of Chemistry and Biochemistry, 2014.

(4) Westcott, B. L.; Enemark, J. H. In *Inorganic Electronic Structure and Spectroscopy*; Solomon, E. I., Lever, A. B. P., Eds.; John Wiley and Sons, Inc.: New York, NY, 1999; Vol. 2, p 435-439.

(5) Judd, E. T.; Youngblut, M.; Pacheco, A. A.; Elliott, S. J. Direct Electrochemistry of Shewanella oneidensis Cytochrome c Nitrite Reductase: Evidence of Interactions across the Dimeric Interface *Biochemistry* **2012**, *51*, 10175-10185.

(6) Fultz, M. L.; Durst, R. A. Mediator compounds for the electrochemical study of biological redox systems: a compilation *Anal. Chim. Acta* **1982**, *140*, 1-18.

(7) Stein, N.; Love, D.; Judd, E. T.; Elliott, S. J.; Bennett, B.; Pacheco, A. A. Correlations between the electronic properties of *Shewanella oneidensis* cytochrome *c* nitrite reductase (ccNiR) and its structure: effects of heme oxidation state and active site ligation *Biochemistry* **2015**, *54*, 3749-3758.